Journal of Advanced Ceramics
2013, 2(4): 347–352
DOI: 10.1007/s40145-013-0082-9

ISSN 2226-4108
CN 10-1154/TQ

Research Article

Synthetic process and spark plasma sintering of $SrIrO_3$ composite oxide

Yongshang TIAN[a,b], Yansheng GONG[a,b,*], Zhaoying LI[a], Feng JIANG[a], Hongyun JIN[a,b]

[a]*Faculty of Material Science and Chemistry*, *China University of Geosciences*, *Wuhan 430074*, *People's Republic of China*
[b]*Engineering Research Center and Application of Nano-Geomaterials of Ministry of Education*, *China University of Geosciences*, *Wuhan 430074*, *People's Republic of China*

Received: July 08, 2013; Revised: September 01, 2013; Accepted: September 07, 2013

Abstract: Single phase of $SrIrO_3$ powders and ceramics were obtained by solid-state chemical reaction method and spark plasma sintering (SPS) technique, respectively. Phase evolutions, characteristics, morphology and resistivity of the samples were studied by using thermogravimetric analysis–differential scanning calorimetry (TG–DSC), X-ray diffractometry (XRD), field emission scanning electron microscopy (FESEM) and four-point probe method, respectively. The results showed that the reaction process to form $SrIrO_3$ phase occurred between $SrCO_3$ and IrO_2 directly during the heating process. By using optimum fabrication conditions established from the TG–DSC results, single phase of $SrIrO_3$ powders was synthesized at 800–1000 ℃. $SrIrO_3$ ceramics were sintered by SPS technique at 1000–1100 ℃ with a pressure of 30 MPa, showing a high relative density of 92%–96% and dense microstructure. The room-temperature resistivity of $SrIrO_3$ ceramics was about 2×10^{-4} Ω·m. The present study can provide high-quality ceramic target for the preparation of $SrIrO_3$ films in traditional physical vapor deposition (PVD) method.

Keywords: $SrIrO_3$; powder; controllable synthesis; spark plasma sintering (SPS)

1 Introduction

Iridium oxide (IrO_2) has been applied as electrode and electrical conducting paste due to its excellent electrical conductivity. However, IrO_2 has a high volatility in air atmosphere due to the formation of volatile IrO_3 phase at high temperature (above 800 ℃), resulting in the degeneration of electrode [1,2]. In recent years, the 4*d*- and 5*d*-electron transition metal oxides (TMOs), e.g., the ruthenates and iridates, have received growing attention for their potential application in catalysis, electrochemistry and microelectronic devices [3–6]. The alkaline-earth iridates $AIrO_3$ (where A is the alkaline-earth element Ca, Sr or Ba) is an important system in oxide iridates [2,7], which can suppress the volatile nature of IrO_2 at high temperature.

* Corresponding author.
E-mail: gongyansheng@hotmail.com

According to McDaniel and Schneider's study on the equilibrium phase diagram of Sr–Ir–O in 1971, Sr–Ir–O compounds have three stable phases: Sr_4IrO_6, Sr_2IrO_4 and $SrIrO_3$ [8], whereas $SrIrO_3$ decomposes to Sr_2IrO_4 and Ir at 1205 ℃; Sr_2IrO_4 decomposes to Sr_4IrO_6 and Ir at 1445 ℃; Sr_4IrO_6 decomposes to SrO and Ir above 1540 ℃ [9]. $SrIrO_3$ has a monoclinic distorted hexagonal $BaTiO_3$ structure with a space group $C2/c$ and lattice parameters of $a = 0.5604$ nm, $b = 0.9618$ nm, $c = 1.4170$ nm and $\beta = 93.26°$ [10] at room temperature under atmospheric pressure.

Most studies among $SrIrO_3$ compound have been focused on thin film preparation by sol–gel, sputtering, pulse laser ablation, and so on [1,6,11–13]. Orthorhombic $SrIrO_3$ perovskite has also been synthesized at a high pressure (5 GPa), and its unusual magnetic characteristics are reported [7]. However, the synthesized processes of $SrIrO_3$ powders and its intrinsic properties, such as the electrical properties of $SrIrO_3$ sintered bulk bodies, have rarely been reported.

So far, dense sintered bodies of alkaline-earth iridates are still difficult to be obtained due to the evaporation of volatile oxide species (IrO_4/IrO_3) in conventional sintering process. For the purpose of application, a very dense ceramic is required. Spark plasma sintering (SPS) technique may consolidate alkaline-earth ruthenates or iridates bodies because the fast heating rate in SPS process may avoid the evaporation of volatile oxide species. Keawprak *et al*. [14] reported the thermoelectric properties of Sr–Ir–O compounds by SPS technique at 1100 ℃, showing a 81.5% relative density of $SrIrO_3$ body, indicating the feasibility of SPS in alkaline-earth iridates compound sintering. However, the relative density of $SrIrO_3$ body still needs to be improved and the SPS process of $SrIrO_3$ ceramics also needs to be further studied.

In the present work, the synthesized conditions of pure $SrIrO_3$ powders derived by solid-state chemical reaction method were studied in detail. In addition, SPS technique was employed to increase the ceramic density, and the effect of sintering temperature on crystal structure, microstructure and resistivity of $SrIrO_3$ ceramics were reported.

2 Experiment

$SrIrO_3$ powders were synthesized by using conventional solid-state chemical reaction method. Strontium carbonate ($SrCO_3$, 99.9%) and iridium oxide (IrO_2, 86.0%) were used as the raw materials. Stoichiometric mixed powders were ground more than half an hour in an agate mortar, then placed into a muffle furnace (JML-5.4-1.6), and calcined for 9 h at a specific temperature. The synthesized powders were removed into a graphite die (Φ10 mm) and sintered in an SPS equipment (SPS-1050). The sintering temperature was from 900 ℃ to 1050 ℃ for 10 min with a uniaxial pressure of 30 MPa and a heating rate of 150 ℃/min. The carbon diffusion layers on the $SrIrO_3$ ceramic surface were removed to avoid any contamination before different detection.

The crystal structure and phase composition were examined by X-ray diffraction (XRD, X'Pert PRO) with Cu Kα radiation at room temperature. Field emission scanning electron microscopy (FESEM, SUV-1080) was used to characterize the morphology of $SrIrO_3$ powders and ceramics. The cumulative distribution of $SrIrO_3$ particles was tested by laser particle size analyzer (JL-1155). The density of ceramics was measured by the Archimedes immersion method. The room-temperature electrical resistivity of the $SrIrO_3$ ceramics was measured by Hall test system (Accent HL 5500 PC).

3 Results and discussion

Figure 1 shows the $SrCO_3$ powders' thermogravimetric (TG) curve and thermogravimetric analysis–differential scanning calorimetry (TG–DSC) curves (at the heating rate of 20 ℃/min in atmosphere) of $SrCO_3$ and IrO_2 mixed powders with mole ratio ($R_{Ir/Sr}$) of 1. From TG–DSC curves of the as-mixed powders, it could be seen that evaporation of free water occurrs below 150 ℃, corresponding to a 0.97% weight loss; the reaction between $SrCO_3$ and IrO_2 to form single-phase $SrIrO_3$ is observed from three exothermic peaks at about 150 ℃ to 850 ℃ with a 12.62% weight loss. No apparent peak and weight loss can be observed at the temperature over 800 ℃. In addition, from the $SrCO_3$ powders' TG curve, it can be deduced that the reaction process to form $SrIrO_3$ phase occurs between $SrCO_3$ and IrO_2 directly, since there is no endothermic peak of the decomposition of $SrCO_3$ during the heating process. From the TG–DSC curves, the proper synthesized temperature of $SrIrO_3$ powders is about 800 ℃.

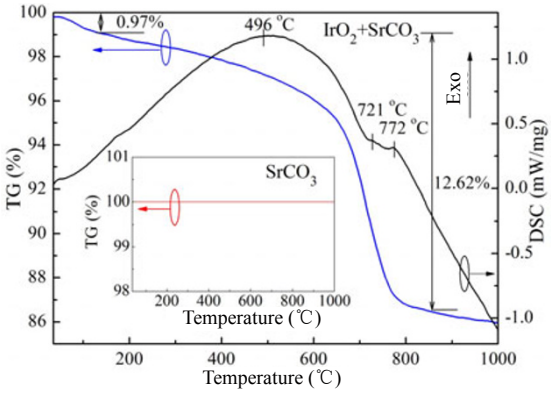

Fig. 1 TG–DSC curves for mixed powders of $SrCO_3$ and IrO_2 at $R_{Ir/Sr}$=1. The inset shows the $SrCO_3$ powders' TG curve.

Figure 2 shows the XRD patterns of synthesized $SrIrO_3$ powders at a calcination temperature of 800–1000 ℃ with $R_{Ir/Sr}=1$. The standard XRD pattern of $SrIrO_3$ is also shown in Fig. 2 for comparison. Every peak in the patterns at the temperature from 800 ℃ to 1000 ℃ can be attributed to $SrIrO_3$ phase. This indicates that the powders are single phase of monoclinic $SrIrO_3$, which starts to form from about 800 ℃ and is in accordance with the TG–DSC results. Some of the peaks are not obvious at the temperature of 800 ℃, while all the characteristic peaks appear and the intensity of the diffraction peaks improves with increasing calcination temperature. The appropriate temperature of synthesizing $SrIrO_3$ powders is identified at 850 ℃ and the lattice parameters of synthesized $SrIrO_3$ are $a=0.5617$ nm, $b=0.9621$ nm, $c=1.4089$ nm, and $\beta=93.30°$, which is calculated according to the XRD results of synthesized $SrIrO_3$ powders at 850 ℃.

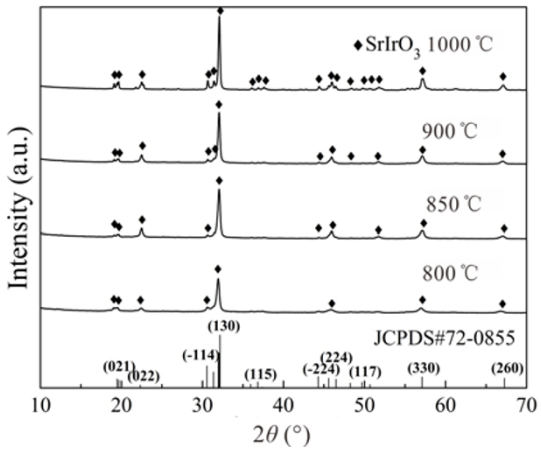

Fig. 2 XRD patterns of synthesized $SrIrO_3$ powders at different calcination temperatures.

Figure 3 presents the FESEM image of $SrIrO_3$ powders, which was synthesized at 850 ℃ and dispersed by ultrasound in alcohol for 30 min. It could be seen that the particle size of $SrIrO_3$ powders is almost uniform, showing a particle size of about 0.4 μm. The cumulative distribution of $SrIrO_3$ particles with different size is shown in Fig. 4. The particle size distribution obeys normal distribution through differential calculation, and the calculated particle sizes of D_{50} and D_{AV} are 0.75 μm and 1.21 μm, respectively, which are a little higher than the FESEM image.

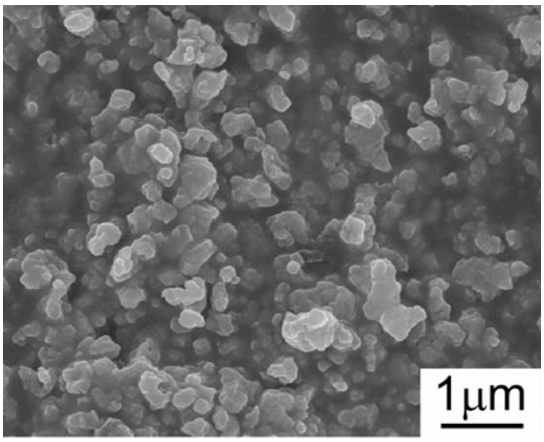

Fig. 3 FESEM image of synthesized $SrIrO_3$ powders at 850 ℃.

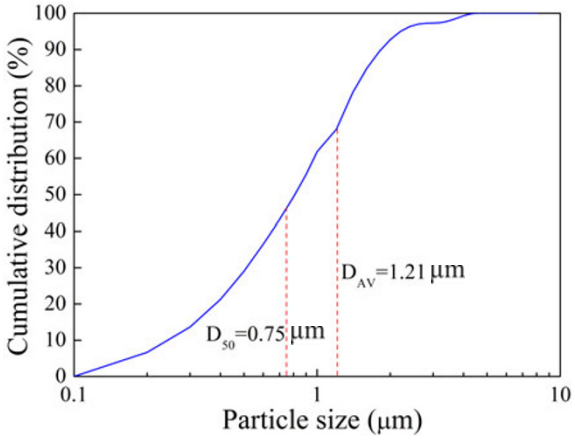

Fig. 4 The cumulative distribution of synthesized $SrIrO_3$ powders at 850 ℃.

Figure 5 shows the XRD patterns of $SrIrO_3$ ceramics by SPS technique at the sintering temperature of 1000–1100 ℃ under a uniaxial pressure of 30 MPa. From the patterns, it can be found that the main diffraction peaks are consistent well with JCPDS card 72-0855 for $SrIrO_3$. Compared with $SrIrO_3$ powders,

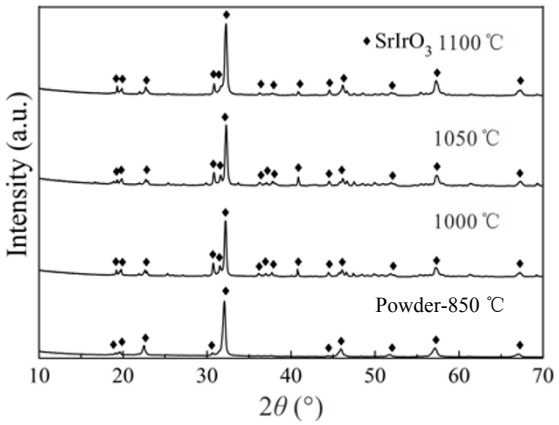

Fig. 5 XRD patterns of $SrIrO_3$ ceramics by SPS technique at different conditions.

the crystallinity of $SrIrO_3$ ceramics are significantly strengthened.

Figure 6 presents the FESEM images of $SrIrO_3$ ceramic fracture surface sintered at 1000–1100 ℃ by SPS technique. The relative densities of $SrIrO_3$ ceramics sintered at 1000 ℃, 1050 ℃ and 1100 ℃ are 93.9%, 96.2% and 92.7%, respectively, which are much denser than the literature [14]. From the FESEM images, it could be seen that a dense structure forms and the average grain size is about 0.6–1.0 μm in length, indicating that the grain growth is slight in comparison with the grain size of the $SrIrO_3$ powders. However, there still exist some nanoscale grains in the sintered bodies. The proper sintering temperature of $SrIrO_3$ ceramics is fixed at 1050 ℃ according to the relative densities.

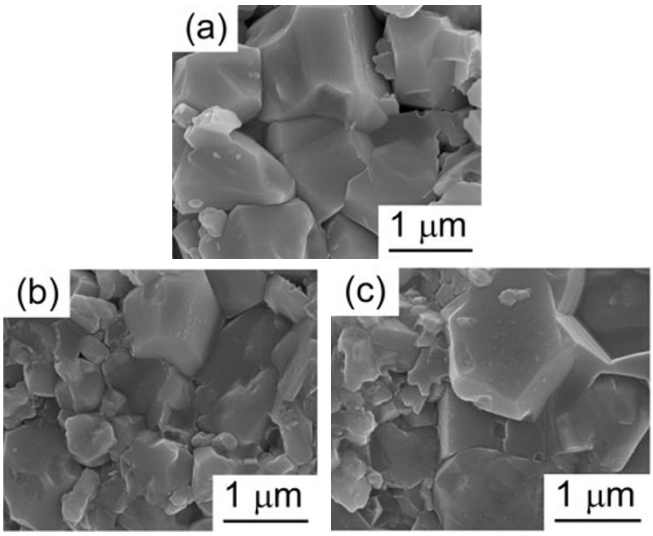

Fig. 6 FESEM images of $SrIrO_3$ ceramic fracture surface sintered at 30 MPa and (a) 1000 ℃, (b) 1050 ℃, (c) 1100 ℃ by SPS technique.

Figure 7 shows the typical sintering displacement and heating curves of the $SrIrO_3$ ceramics with sintering time variation. At the initial stage, the powders are swelled with increasing temperature, while the powders are contracted rapidly with the intervention of pressure. In the heating preservation stage, the densification of $SrIrO_3$ ceramics is almost finished above 900 ℃. Figure 8 shows the shrinking rate of $SrIrO_3$ ceramics with the variation of sintering temperature in SPS process. The low or high speed of powder expansion and ceramic contraction could be found from the shrinking rate curve. The variation of shrinking rate below 600 ℃ is due to the powder expansion, which is caused by the increasing temperature and the powder inherent expansion properties. When the pressure gradually adds to 30 MPa, the shrinking rate increases significantly with increasing sintering temperature, which starts from 700 ℃ and ends at 920 ℃. After that, the densification process reaches to the balance. All the processes are consistent with sintering displacement and heating

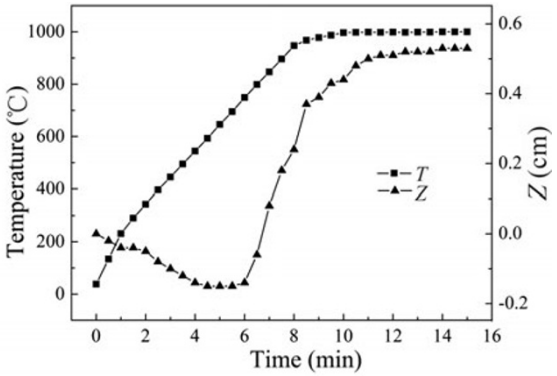

Fig. 7 Typical sintering displacement and heating curves of the $SrIrO_3$ ceramics by SPS technique.

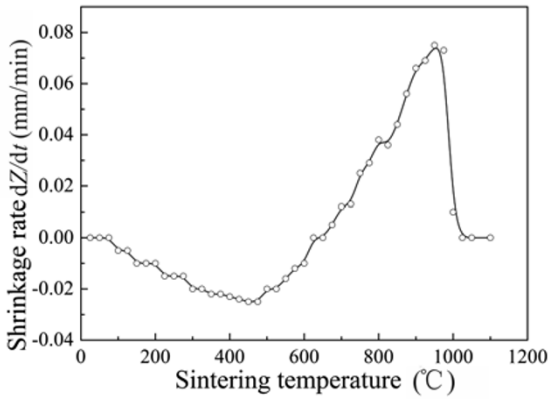

Fig. 8 Shrinkage rate of $SrIrO_3$ ceramics sintered by SPS with increasing sintering temperature.

curves of sintering $SrIrO_3$ ceramics (Fig. 7), and the density of $SrIrO_3$ ceramics reaches the maximum at the setting condition.

The room-temperature electrical resistivity and Ir/Sr ratio ($R_{Ir/Sr}$) of $SrIrO_3$ ceramics are shown in Table 1. The results of $R_{Ir/Sr}$ were obtained by energy-dispersive spectrometer (EDS), showing a nearly stoichiometric ratio at the sintering temperature of 1000–1100 ℃. The nonstoichiometric ratio may due to the volatility of iridium oxide at high sintering temperature. The electrical resistivity is about 2×10^{-4} Ω·m, showing a little higher value than the literature [14,15], which is probably due to the coulomb-scattering mechanism on carrier at the boundary causing by the smaller grains (Fig. 6) [16]. In addition, the SPS $SrIrO_3$ ceramics in the present study show a high relative density and dense microstructure, which could be used as a ceramic target to satisfy the demand of preparation of $SrIrO_3$ films in physical vapor deposition (PVD) method.

Table 1 Relative density, $R_{Ir/Sr}$ and electrical resistivity of $SrIrO_3$ ceramics

Temperature (℃)	Relative density (%)	$R_{Ir/Sr}$	Bulk resistivity (10^{-4}Ω·m)
1000	93.9	0.953	2.049
1050	96.2	0.989	2.032
1100	92.7	0.946	2.194

4 Conclusions

In the current work, nearly stoichiometric $SrIrO_3$ powders and ceramics were obtained by solid-state chemical reaction method and SPS technique, respectively. $SrIrO_3$ powders could be synthesized through the reaction of $SrCO_3$ and IrO_2 in a wide range of temperature (800–1000 ℃). With increasing calcination temperature, the crystallinity of the as-prepared $SrIrO_3$ powders was improved significantly. The optimum SPS condition for the dense $SrIrO_3$ ceramics was 1050 ℃ with a pressure of 30 MPa, showing a relative density of about 96.2% and electrical resistivity of about 2×10^{-4} Ω·m.

Acknowledgements

This work was financially supported by Hubei Provincial Nature Science Found of China (2011CDB331), State Key Laboratory of Advanced Technology for Materials Synthesis Processing (Wuhan University of Technology, 2012-KF-3), and the Fundamental Research Founds for National University, China University of Geosciences (Wuhan) (CUG120118).

References

[1] PauPorté T, Aberdam D, Hazemann J-L, *et al*. X-ray absorption in relation to valency of iridium in sputtered iridium oxide films. *J Electroanal Chem* 1999, **465**: 88–95.

[2] Keawprak N, Tu R, Goto T. Thermoelectricity of $CaIrO_3$ ceramics prepared by spark plasma sintering. *J Ceram Soc Jpn* 2009, **117**: 466–469.

[3] Xu W, Zheng L, Xin H, *et al*. $BaRuO_3$ thin films prepared by pulsed laser deposition. *Mater Lett* 1995, **25**: 175–178.

[4] Choi KJ, Baek SH, Jang HW, *et al*. Phase-transition temperatures of strained single-crystal $SrRuO_3$ thin films. *Adv Mater* 2010, **22**: 759–762.

[5] Cao G, Durairaj V, Chikara S, *et al*. Non-Fermi-liquid behavior in nearly ferromagnetic $SrIrO_3$ single crystals. *Phys Rev B* 2007, **76**: 100402.

[6] Liu Y, Masumoto H, Goto T. Structural, electrical and optical characterization of $SrIrO_3$ thin films prepared by laser-ablation. *Mater Trans* 2005, **46**: 100–104.

[7] Zhao JG, Yang LX, Yu Y, *et al*. High-pressure synthesis of orthorhombic $SrIrO_3$ perovskite and its positive magnetoresistance. *J Appl Phys* 2008, **103**: 103706.

[8] McDaniel CL, Schneider SJ. Phase relation in the $SrO–IrO_2–Ir$ system in air. *J Res NBS A Phys Ch* 1971, **75A**: 185–196.

[9] Jacob KT, Okabe TH, Uda T, *et al*. Phase relations in the system Sr–Ir–O and thermodynamic measurements on $SrIrO_3$, Sr_2IrO_4 and Sr_4IrO_6 using solid-state cells with buffer electrodes. *J Alloys Compd* 1999, **288**: 188–196.

[10] Longo JM, Kafalas JA, Arnott RJ. Structure and properties of the high and low pressure forms of $SrIrO_3$. *J Solid State Chem* 1971, **3**: 174–179.

[11] Sumi A, Kim YK, Oshima N, *et al*. MOCVD growth of epitaxial $SrIrO_3$ films on (111) $SrTiO_3$ substrates. *Thin Solid Films* 2005, **486**: 182–185.

[12] Jang SY, Kim H, Moon SJ, *et al*. The electronic structure of epitaxially stabilized 5*d* perovskite $Ca_{1-x}Sr_xIrO_3$ ($x = 0$, 0.5, and 1) thin films: The role of strong spin-orbit coupling. *J Phys*: *Condens Matter* 2010, **22**: 485602.

[13] Jang SY, Moon SJ, Jeon BC. PLD growth of epitaxially-stabilized 5*d* perovskite $SrIrO_3$ thin films. *J Korean Phys Soc* 2010, **56**: 1814–1817.

[14] Keawprak N, Tu R, Goto T. Thermoelectric properties of Sr–Ir–O compounds prepared by spark plasma sintering. *J Alloys Compd* 2010, **491**: 441–446.

[15] Qasim I, Kennedy BJ, Avdeev M. Synthesis, structures and properties of transition metal doped $SrIrO_3$. *J Mater Chem A* 2013, **1**: 3127–3132.

[16] Zhang J, Tu R, Goto T. Fabrication of transparent SiO_2 glass by pressureless sintering and spark plasma sintering. *Ceram Int* 2012, **38**: 2673–2678.